Supplementary Information

Model-independent measurement of the charge density in an Fe atom probe needle using off-axis electron holography without mean inner potential effects

Vadim Migunov, Andrew London, Michael Farle and Rafal E. Dunin-Borkowski

1 Off-axis electron holograms acquired at different applied voltages

Off-axis electron holograms were acquired in Lorentz mode using elliptical illumination with the biprism voltage set to $V_{BP} = 130$ V. A representative hologram is shown in Fig. 1. Only the the tip of the APT needle was found to be transparent to the electron beam. Reconstruction of holograms was performed by Fourier transformation and filtering of the sideband using a Butterworth filter with a size of approximately $(10.4\ \mathrm{nm})^{-1}$, before centering the sideband, inverse Fourier transformation and calculating the amplitude and phase.

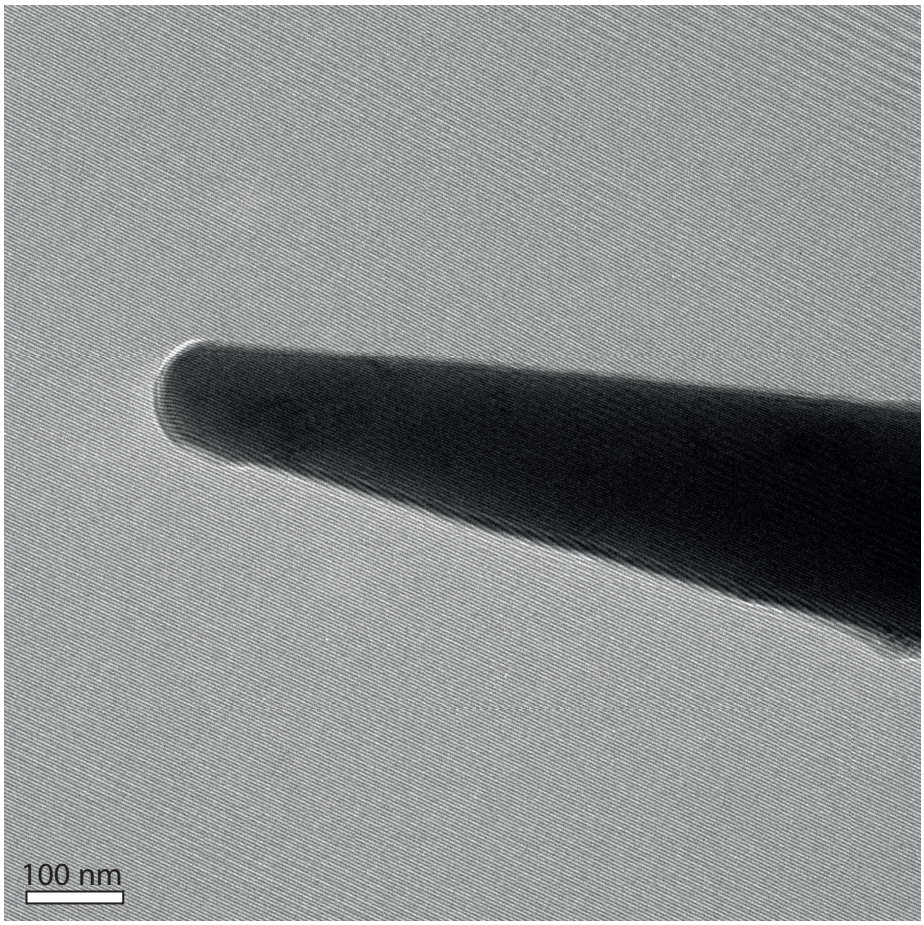

Figure 1: Representative off-axis electron hologram acquired in Lorentz mode at a specimen tilt angle of $\alpha = 5\ ^\circ$ and an applied bias voltage of $V_B = 0$ V.

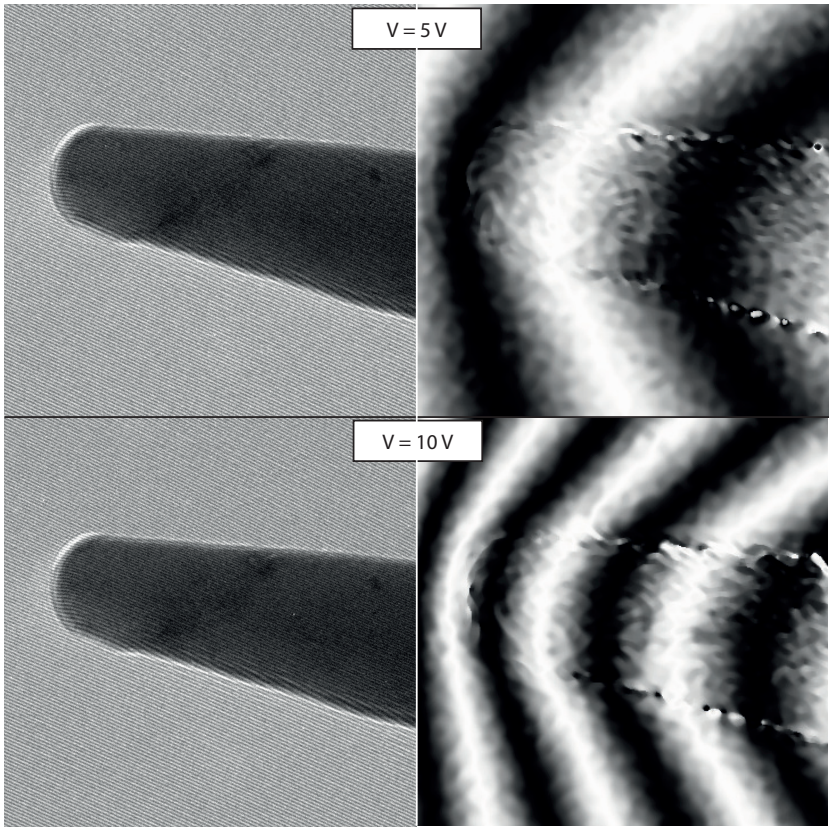

Figure 2: Central regions of holograms (left) and 1× amplified cosines of the reconstructed phase (right) of the atom probe needle acquired at a specimen tilt angle of $\alpha = 5°$ and at the applied bias voltages indicated. In the phase contour maps (right), the 0 V hologram was used as a reference hologram to subtract the mean inner potential and magnetic contributions to the phase.

Central regions of holograms acquired at different applied bias voltages and cosines of corresponding reconstructed phase images (after subtracting the mean inner potential contribution to the phase) are shown in Figs. 2 and 3. Strong bending of the interference fringes is visible at higher applied voltages (30 and 40 V). At these voltages, the recorded phase images suffer from additional distortions, which result in imperfect subtraction of the mean inner potential contribution to the phase (see Fig. 3).

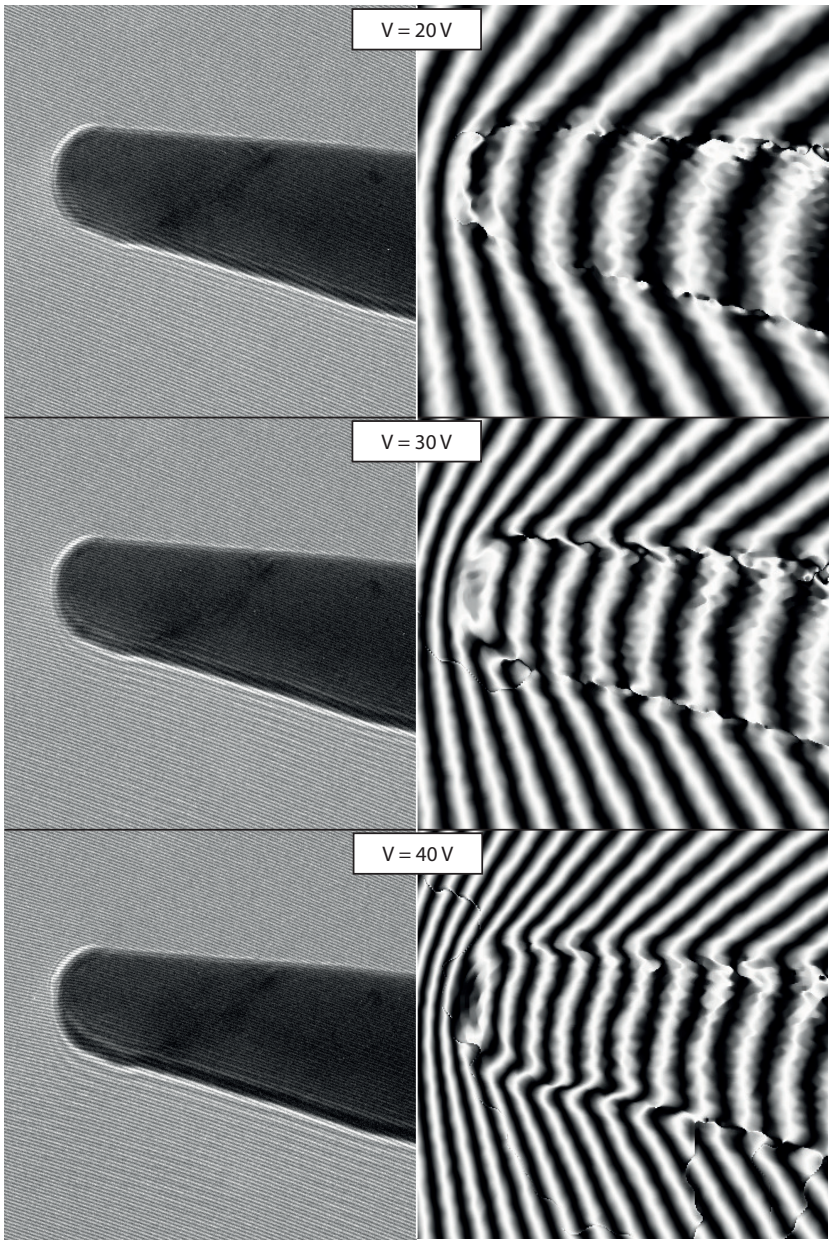

Figure 3: Central regions of holograms (left) and 1× amplified cosines of the reconstructed phase (right) of the atom probe needle acquired at a specimen tilt angle of $\alpha = 5°$ and at the applied bias voltages indicated. In the phase contour maps (right), the 0 V hologram was used as a reference hologram to subtract the mean inner potential and magnetic contributions to the phase.

2 Off-axis electron holograms acquired at different specimen tilt angles

Central regions of electron holograms acquired at different specimen tilt angles and cosines of corresponding reconstructed phase images (after subtracting the mean inner potential contribution to the phase) are shown in Fig. 4. The images highlight the fact that the needle has close-to-cylindrical symmetry.

3 Sensitivity of the model-independent approach to noise

Since the model-independent measurement of charge density requires the calculation of phase derivatives, it is sensitive to noise in the phase images. In order to assess the influence of noise, four phase images were simulated corresponding to line charges with constant charge densities, for a total charge of -5 e^-, +12.5 e^-, -12.5 e^- and +5 e^- (see Fig. 5a). Gaussian noise with mean μ and standard deviation σ was added (see Figs. 5c-e). Charge density profiles were calculated from each image. The presence of noise was found to result in an increase in uncertainty in charge density measurement and even in the apparent absence of an uncharged region between positions 237 and 265 in the green curve in the graph shown in Fig. 5.

4 Sensitivity of the model-independent approach to a magnetic field

Figure 6 shows the apparent projected charge density distribution that would be inferred by applying the model-independent contour integration approach to

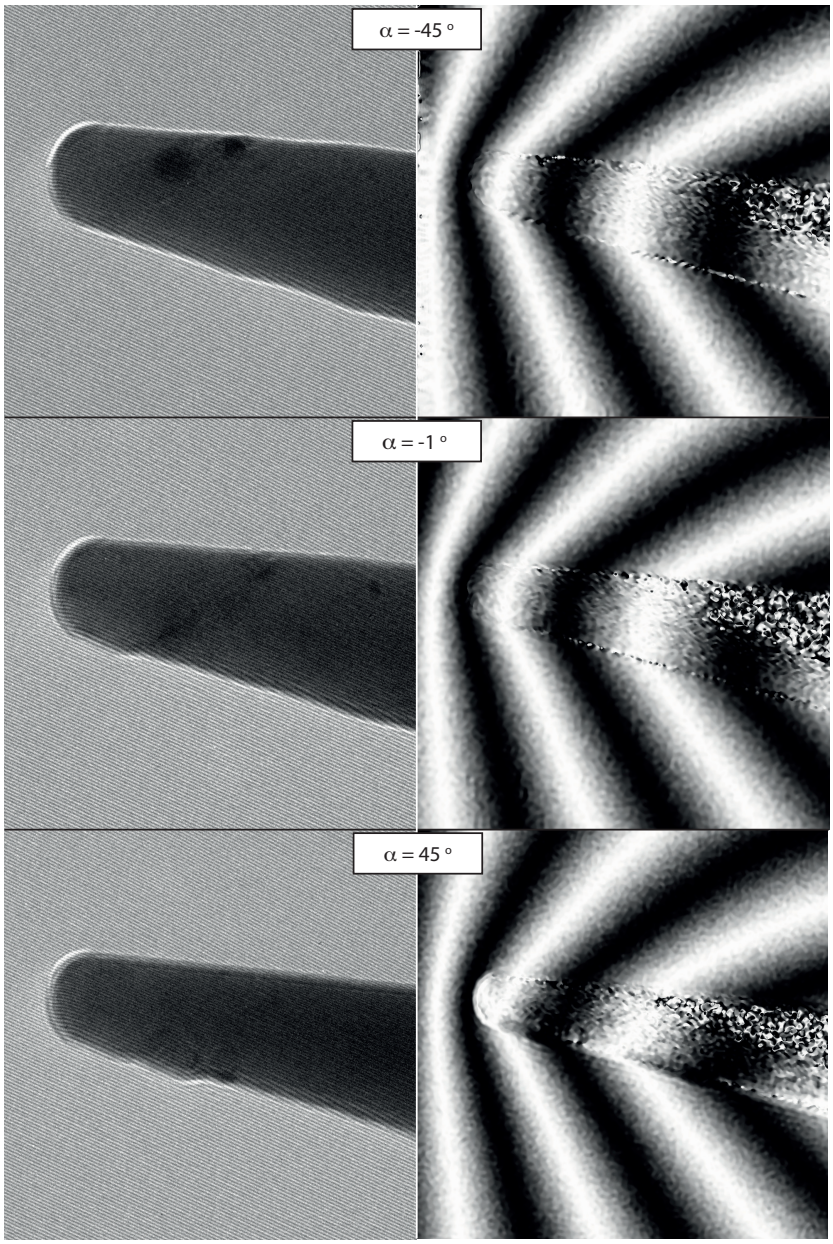

Figure 4: Central regions of holograms (left) and 1× amplified cosines of the reconstructed phase (right) of the atom probe needle acquired at different specimen tilt angles α and at an applied bias voltage of 5 V.

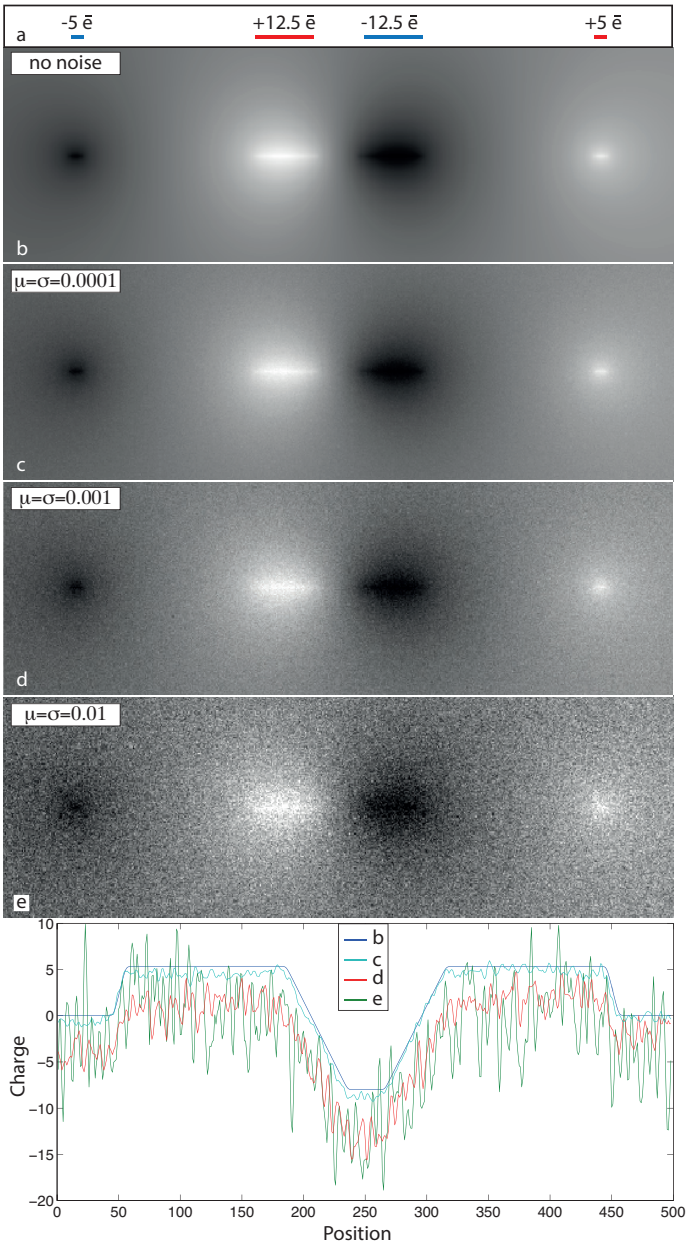

Figure 5: (a) Schematic diagram showing the charge distribution used to simulate the phase images shown in (b-e). Red and blue lines represent lines of constant positive and negative charge density, respectively. The total amount charge in each line is indicated. (b-e) show corresponding phase images with different amounts of noise with mean μ and standard deviation σ. The graph shows the corresponding inferred cumulative charge profiles. The lateral position is given in arbitrary units.

the magnetic phase shift of a uniformly magnetised sphere. The presence of an apparent charge distribution inside the sphere highlights the fact that the magnetic contribution to the phase shift must be subtracted from a recorded phase image before measuring the charge density using the contour integration approach. The fact that this subtraction is necessary can be illustrated analytically for a uniformly magnetised sphere, for which the magnetic phase shift inside ϕ_{int} and outside ϕ_{ext} the sphere can be expressed by the expressions [1, 2, 3]

$$\phi_{int}(x,y) = \frac{2}{3}\mu_0 R^3 \left(\frac{e}{\hbar}\right)\left(\frac{M_y x - M_x y}{x^2+y^2}\right)\left[1-\left(1-\left(\frac{x^2+y^2}{R^2}\right)\right)^{\frac{3}{2}}\right] \tag{1}$$

$$\phi_{ext}(x,y) = \frac{2}{3}\mu_0 R^3 \left(\frac{e}{\hbar}\right)\left(\frac{M_y x - M_x y}{x^2+y^2}\right) \tag{2}$$

where R is the radius of the sphere, e is an elementary charge, $\hbar$ is the reduced Planck constant, μ_0 is the vacuum permeability and M_x and M_y are the components of magnetisation inside the sphere perpendicular to the incident electron beam direction. The corresponding Laplacian of the phase, whose integration across the field of view is equivalent to the contour integration approach discussed in the main text, can be expressed analytically in the form

$$\nabla^2\phi_{int}(x,y) = \frac{24}{3}\mu_0\left(\frac{e}{\hbar}\right)\frac{\left(x^2+y^2-R^2\right)\left(M_y x - M_x y\right)}{R^3} \tag{3}$$

$$
\begin{aligned}
\nabla^2\phi_{ext}(x,y) =& \frac{4}{3}\mu_0 R^3 \left(\frac{e}{\hbar}\right) \times \\
& \left(\frac{y\left(y^2-3x^2\right)M_x + x\left(x^2-3y^2\right)M_y}{(x^2+y^2)^3} \right. \\
& \left. + \frac{y\left(3x^2-y^2\right)M_x + x\left(3y^2-x^2\right)M_y}{(x^2+y^2)^3} \right) \equiv 0.
\end{aligned} \tag{4}
$$

These equations illustrate the fact that the Laplacian of the magnetic phase shift inside the boundary of the sphere is not equal to 0 (except for where $M_x y = M_y x$). Figure 7 shows the corresponding Laplacian of the magnetic phase shift calculated for a uniformly magnetised sphere of radius $R = 350$ px, calculated using Eqs. 3 and 4.

5 Insensitivity of the "three-region" model to charge outside the field of view

Figure 8 illustrates, in the form of simulations for the model based on three collinear lines of charge discussed in the manuscript, the insensitivity of the electrostatic potential and electric field to the total length of the needle $L = 2c_0$, *i.e.*, to the presence of charge outside the field of view .

6 Three-dimensional electrostatic potential

Figure 9 shows the three-dimensional electrostatic potential inferred from the charge distribution measured in the manuscript. Figure 10 shows a comparison of the electrostatic potential and electric field obtained using the "3-region" model (left) and a single line charge (right), as described in the manuscript. The equipotential lines are closer to the surface of the needle for the "3-region" model.

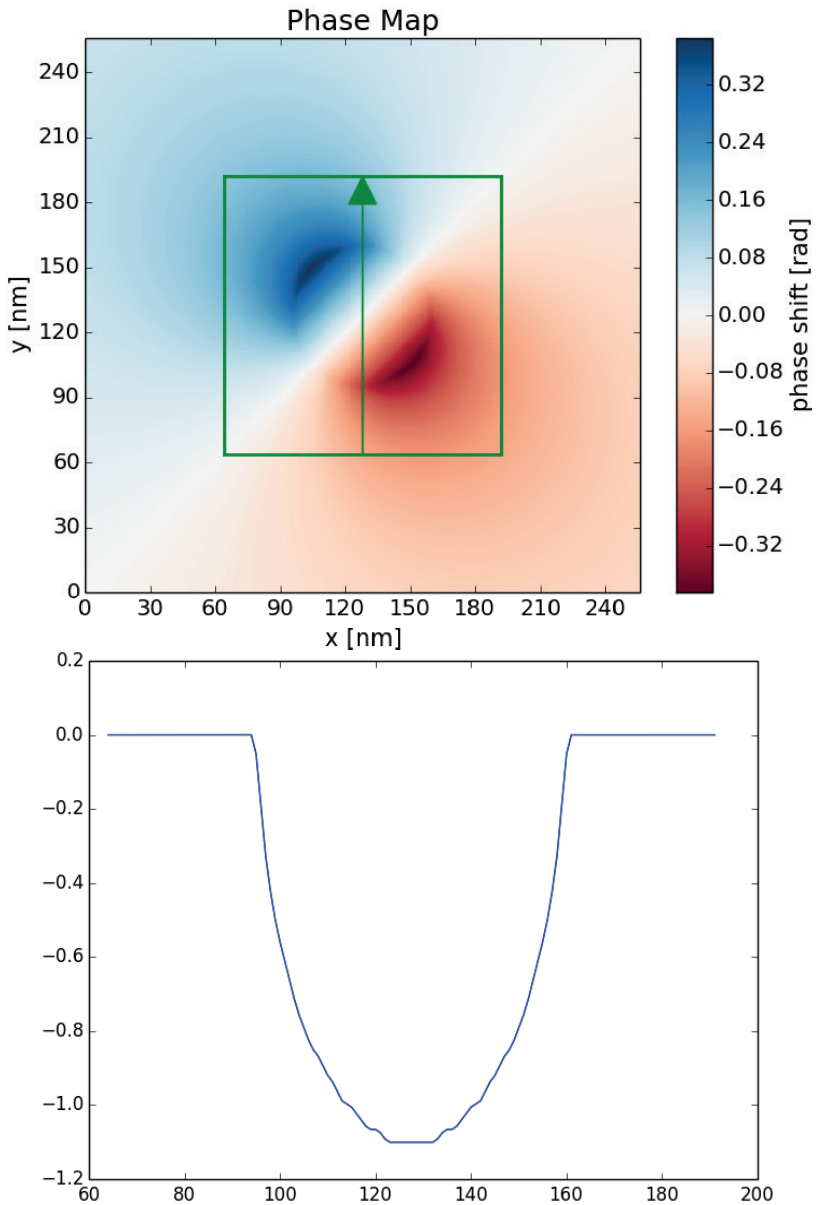

Figure 6: Simulated magnetic phase shift of a uniformly magnetised sphere and apparent charge density profile obtained by applying the model-independent contour integration approach to this image within the green integration contour.

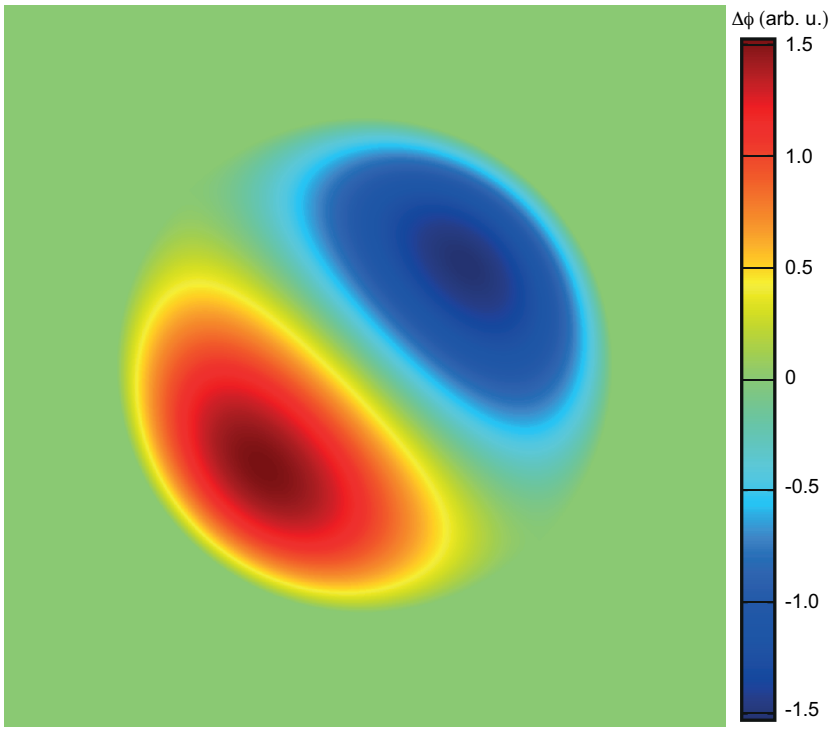

Figure 7: Laplacian of the phase shift of a uniformly magnetised sphere calculated using Eqs. 3 and 4.

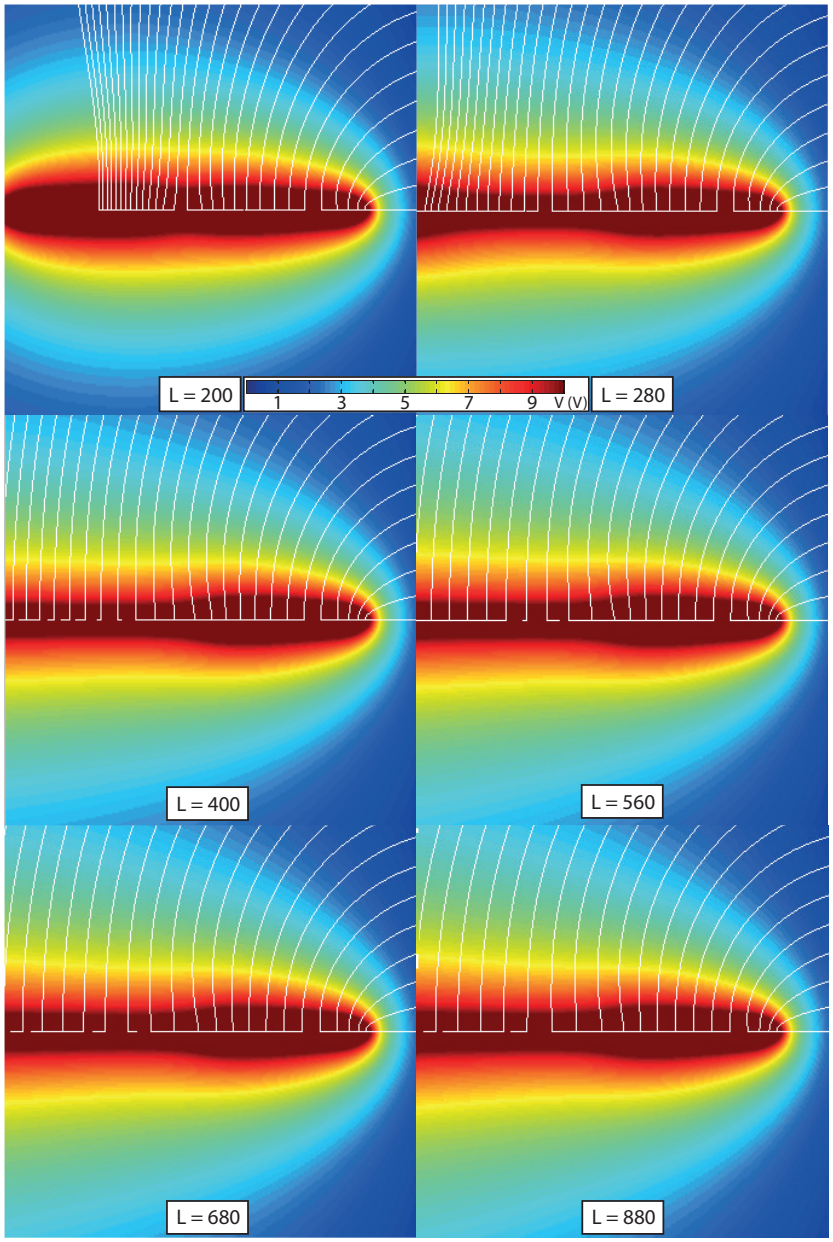

Figure 8: Electrostatic potential (colours) and electric field (white lines) in the plane $z = 0$ simulated for different values of the total needle length L (indicated in pixels). Other parameters are identical to those used in the manuscript. The size of each image is 228 x 228 pixels.

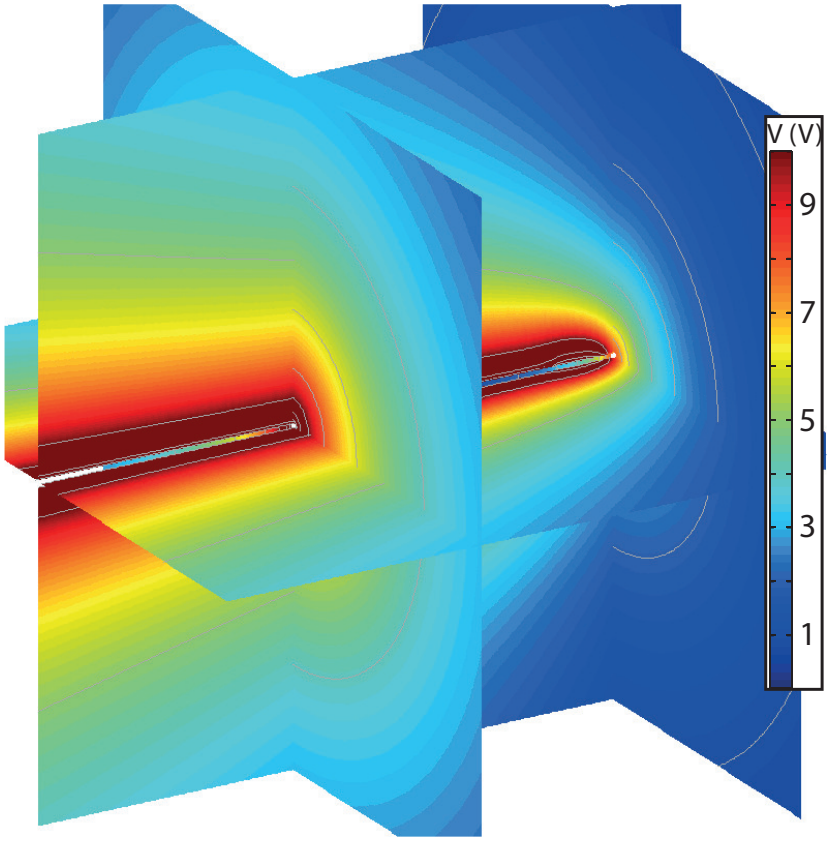

Figure 9: Three-dimensional representation of the electrostatic potential around the needle corresponding to the charge profile determined in the manuscript using the model-independent approach.

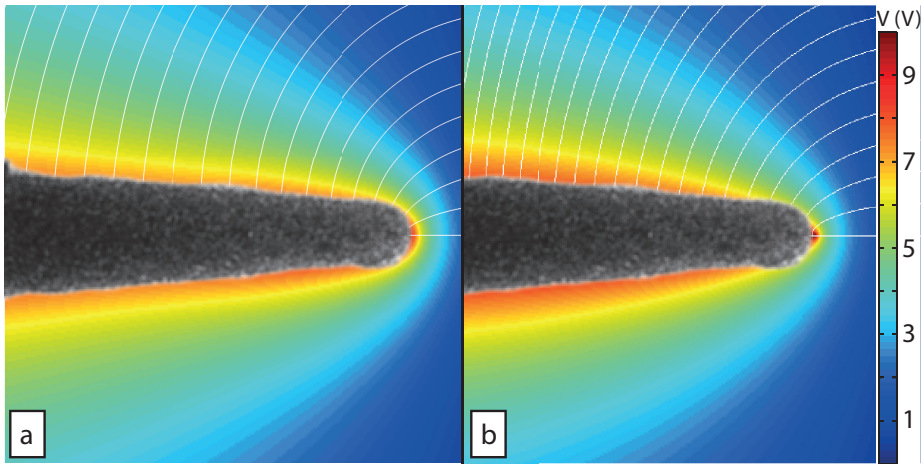

Figure 10: (a) Central slice ($z = 0$) of the electrostatic potential and electric field inferred from a model for the needle that is based on three superimposed charge density profiles (see text for details). (b) Corresponding electrostatic potential and electric field for a single constant charge density profile. In each plot, the white lines correspond to electric field lines and the colours correspond to equipotential contours. The amplitude image of the needle is overlaid.

References

[1] M. De Graef, N. T. Nuhfer, and M. R. McCartney. Phase contrast of spherical magnetic particles. *Journal of Microscopy*, 194(1):84–94, 1999.

[2] I. Antypas. *Theoretical Approaches to Magnetic Induction Mapping in the Transmission Electron Microscope*. PhD thesis, University of Cambridge, 2007.

[3] A. Keimpema. *Electron Holography of Nanoparticles*. PhD thesis, University of Groningen, 2008.